



Biomechanics of traumatic brain injury

Tamer El Sayed^a, Alejandro Mota^a, Fernando Fraternali^b, Michael Ortiz^{a,*}

^aDivision of Engineering and Applied Science, California Institute of Technology, Pasadena, CA 91125, USA

^bDepartment of Civil Engineering, University of Salerno, 84084 Fisciano (SA), Italy

ARTICLE INFO

Article history:

Received 7 February 2008

Received in revised form 12 May 2008

Accepted 15 June 2008

Available online 25 June 2008

Keywords:

Brain tissue damage
Finite deformation
Plasticity
Finite viscoelasticity
Diffuse axonal injury
Cavitation injury
Traumatic brain injury

ABSTRACT

A biomechanical model for traumatic brain injury and soft tissue damage is presented. A variational constitutive model for soft biological tissues is utilized to reproduce axonal damage and cavitation injury through inelastic deformation. The material response is split into elastoplastic and viscoelastic components, including rate effects, shear and porous plasticity, and finite viscoelasticity. Mechanical damage of brain tissue is classified as volumetric (compression/tension) and shear-type. Finite element simulations of brain injuries are presented, examining frontal and oblique head impacts with external objects. Localization, extension, intensity and reversibility/irreversibility of tissue damage are predicted. Future directions of this work, relating mechanical damage and physiological brain dysfunction, and application to relevant medical and engineering problems are discussed.

© 2008 Elsevier B.V. All rights reserved.

1. Introduction

Brain damage resulting from traumatic brain injuries (TBI) under impact/acceleration loading is often classified as *focal* and/or *diffuse* in the medical literature. The first consists of contusions, lacerations, haematomas (extradural or intradural), and tentorial/tonsillar herniation. Focal damage may also occur as *coup* or *contrecoup* (opposite to the site of impact). On the other hand, diffuse damage encompasses *diffuse axonal injury* (DAI), cerebral swelling, cerebral ischemia, and is often associated with focal damage. Alternatively, according to the process that contributes to the neuronal damage after injury, brain damage can be classified as *primary* or *secondary*. Direct (primary) brain injury results from both the direct impact of the brain against the inner contours of the skull and the forces occurring from acceleration, deceleration and rotation of the brain inside the cranium. On the other hand, secondary injury indicates brain damage that occurs within days of the immediate trauma, due to the long-term effects of the impact.

Some of the frequent causes of damage are the relative motion of the brain with respect to the skull (brain retarded or set into motion subsequently by the skull); striking and bouncing of the parenchyma against inner skull protrusions; cavitation phenomena induced by negative pressures (*volumetric or compression–tension damage*); rupture of bridging veins, axonal fibers and vascular tissue (*shear damage*).

Fig. 1 (adapted from Kleiven [17]) shows the dynamics of a frontal impact injury and the associated compression–tension damage. The translational cranial motion causes relative brain movements and short-term intracranial pressure gradients. High positive pressures are observed at the coup site, together with marked negative pressures at the contrecoup site (cf. Lindgreen and Rinder [19], Nahum et al. [28], Johnson and Young [15]). Coup contusions are produced by the slapping effect of the skull hitting the brain; contrecoup lesions follow from the bouncing of the brain against the inner posterior surface of the skull and the possible development of *cavitation bubbles* within the brain due to high negative pressures. The growth and collapse of these bubbles may induce local tissue damage. This phenomenon, known as *contre cavitation*, is well recognized in the literature (cf., e.g., Lubock and Goldsmith [20], Hardy et al. [13]; Nusholtz et al. [29]; Brennen [5]; Johnson and Young [15]).

Cavitation effects can also be observed in the coup region (*coup cavitation*), due to high negative pressures, which immediately follow a severe shock wave front in both the coup and contrecoup areas [12,19,10,35]. Coup lesions are usually prevalent in the case of an impact by a small object, while contrecoup lesions are typically more severe under impact from large objects. The development of coup and/or contrecoup lesions is also dependent on the part of the skull which is impacted. There is some evidence that frontal impacts always result in frontal lobe injuries and that occipital and temporal impacts cause prevalent contrecoup lesions (cf. Leestma [18]). However, in many cases, both coup and contrecoup lesions are observed.

* Corresponding author.

E-mail address: ortiz@aero.caltech.edu (M. Ortiz).

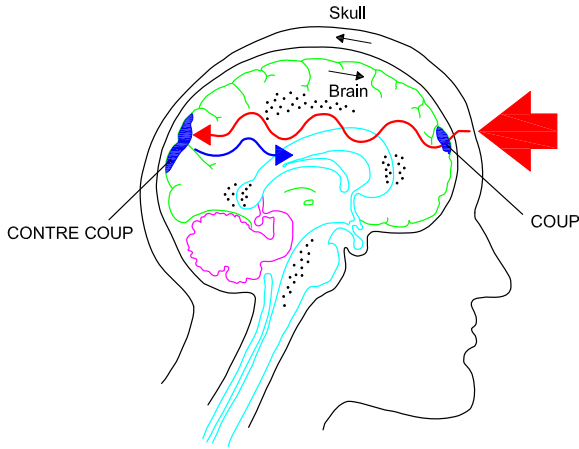


Fig. 1. Coup–contrecoup injury (adapted from Kleiven [17]).

Shear damage is mainly produced by rotational movements of the parenchyma within the skull (angular acceleration injuries) and bending/stretching of the craniospinal junction [1]. This type of trauma is often associated with DAI, since rotational or bending motions may lead to severe shearing of axons in different brain regions. DAI was defined by Strich in [37], and is now widely recognized in the literature (cf., e.g., Perles and Rewcastle [33], Adams and Graham [1]); it is observed in about 30% of the cases, with varying degrees of severity, in the Glasgow brain trauma database [1]. When DAI occurs, various and widespread regions of the brain may no longer be able to function or intercommunicate.

Biomechanical modeling of traumatic brain injuries requires the formulation of complex constitutive equations, accounting for large strains, time and rate effects, and consistent damage models. The current biomechanical literature is mainly concerned with hyperelastic or finite viscoelastic models, accounting for small perturbations away from thermodynamic equilibrium (see, e.g., Prange and Margulies [34], Miller and Chinzei [23,24], Miller et al. [26], Meaney [21], Brands et al. [3], Brands et al. [4], Velardi et al. [39]). Nevertheless, some constitutive models which include plasticity, hysteresis, permanent deformation, and biphasic (solid/fluid) behavior of soft biological tissues have appeared in recent years [2,7,9,11].

The present study deals with the biomechanical modeling of the brain tissue response to traveling impact waves, and the computational simulation of traumatic brain injuries. The model recently proposed in [7,8] is employed, which is able to reproduce permanent brain tissue damage in the form of plastic sliding between brain layers and irreversible growth of voids or bubbles in the material. These features enable the simulation of DAI and cavitation injury. The model includes time-dependent viscous deformations and large perturbations of the material from thermodynamic equilibrium via an exact finite viscoelasticity theory.

Finite element simulations of two different traumatic brain injuries are presented, examining a frontal (validated) and oblique (predictive) impact events. In the first case, the obtained results were validated against an experiment on the intracranial pressure dynamics in a human cadaver impacted by a rigid mass [28].

In contrast to other available simulations of TBIs which essentially relate brain damage to stress–strain intensity in elastic or viscoelastic finite element models (cf. Zhou et al. [46], Zhang et al. [43,44], Kleiven [17], Kleiven and von Holst [16], Horgan and Gilchrist [14]), the current study attempts to describe brain injuries through effective mechanical damage parameters. This attempt relates the damage to plastic and viscous deformation of the

tissue. Elastoplastic and viscoelastic material responses are combined in parallel to reproduce both permanent (time infinity) and transient damage. Both are of volumetric (tension or cavitation damage) and/or deviatoric (shearing damage) types. The presented TBI simulations include maps of intracranial pressure, shear strain, and mechanical damage parameters. Promising applications of this work to relevant medical and engineering problems are discussed in the closing section.

2. A mechanical model of brain tissue

A useful characterization of the mechanical behavior of brain tissue is supplied by the constitutive model recently proposed in [7,8] for large deformation of soft materials. The model inelastic response is decomposed into equilibrium and non-equilibrium components via an elastoplastic network acting in parallel with several viscoelastic mechanisms. The elastoplastic component describes long-term behavior and permanent material damage, while the viscoelastic ones account for time-dependent viscous dissipation.

A thermodynamical variational approach to the constitutive equations (cf. Ortiz and Stainier [32], Yang et al. [42]) is adopted and the following free energy is introduced:

$$A = W^e(e_j^e, \theta^e) + W^p(e^p, \theta^p) + \sum_{i=1}^M W_i^v(e_{ij}^e, \theta_i^e), \quad (2.1)$$

where $(i = 1, \dots, M)$ is the number of viscoelastic mechanisms; W^e and W_i^v are elastic strain energy densities; W^p is a plastic stored energy; e^e , e_i^e and e^p are elastic and plastic logarithmic shear strains e_j^e and e_{ij}^e ($j = 1, 2, 3$) are the eigenvalues of the elastic logarithmic shear strains \mathbf{e}^e and \mathbf{e}_i^e , respectively, which correspond to the principal stretches; θ^e , θ_i^e and θ^p are elastic and plastic logarithmic volumetric strains, respectively [7,8]. In the following sections, the subscript j indicates eigen-components and ranges over 1,2,3; i refers to the viscoelastic networks and ranges over 1, ..., M ; the superscripts e, p and v denote elastic, plastic and viscous quantities, respectively.

The elastic strain energy W^e rules the elastic part of the elastoplastic response and takes the following form:

$$W^e(e_j^e, \theta^e) = \sum_{j=1}^3 \sum_{r=1}^N \frac{\mu_r}{\alpha_r} ([\exp(e_j^e)]^{\alpha_r} - 1) + \frac{\kappa}{2} (\theta^e)^2, \quad (2.2)$$

where N is the number of Ogden's functions [30] modeling the shear deformation, μ_r and α_r are shear moduli and dimensionless stretch exponents ($r = 1, \dots, N$), and κ is the bulk modulus, characterizing the volumetric deformation. The elastic strain energy densities W_i^v have the same structure.

The plastic stored energy W^p is represented by

$$W^p(e^p, \theta^p) = \frac{n\sigma_0 e_0^p}{n+1} \left(1 + \frac{e^p}{e_0^p}\right)^{\frac{n+1}{n}} + \frac{n\sigma_0 e_0^p}{n+1} N_v \frac{4\pi a^3}{3} g(\theta^p, n), \quad (2.3)$$

where σ_0 is the yield stress, e_0^p is the reference plastic strain, n is the hardening exponent, N_v is the void density per unit undeformed volume of the material, a is the void radius, θ^p is the volumetric plastic strain, and

$$g(\theta^p, n) = \int_1^{1/f} \left(1 + \frac{2}{3e_0^p} \log \frac{x}{x-1 + \frac{f_0}{f_0 + \exp \theta^p - 1}}\right)^{\frac{n+1}{n}} dx \quad (2.4)$$

f_0 and f being the initial and current volume fractions, respectively.

Permanent shear damage of the tissue, as induced by diffuse axonal shearing, is modeled through the first term on the right hand side of (2.3), in the form of irreversible plastic sliding. Cavitation

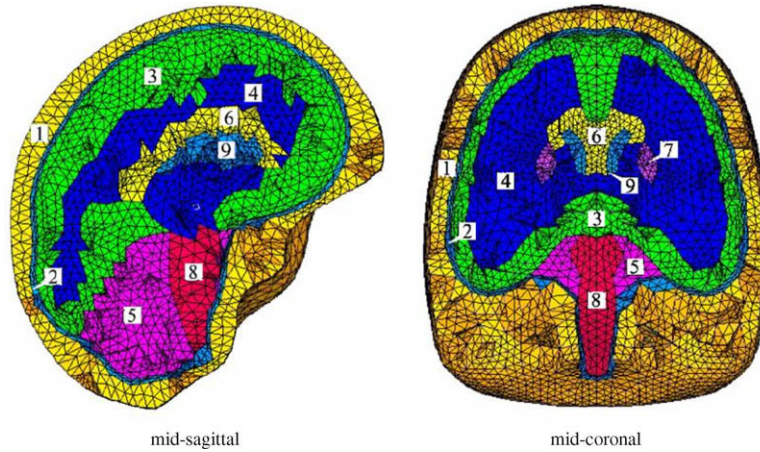


Fig. 2. Mid-sagittal and mid-coronal sections of the adopted head finite element model: (1) skull without facial bones; (2) CSF; (3) gray matter; (4) white matter; (5) cerebellum; (6) corpus callosum; (7) telencephalic nuclei; (8) brain stem and (9) ventricles.

damage, associated with the instable growth of voids in the material is modeled through porous plasticity in the second term on the right hand side of (2.3) [31,40,41].

Rate effects are described through the following dual kinetic potentials:

$$\psi^* = \frac{m^2 \sigma_0 \dot{e}_0^p}{m+1} \left(\frac{\dot{e}^p}{\dot{e}_0^p} \right)^{\frac{m+1}{m}} + \frac{m^2 \sigma_0 \dot{e}_0^p}{m+1} N_v \frac{4\pi a^3}{3} (1 - f_m) \left| \frac{2\dot{a}}{\dot{e}_0^p a} \right|^{\frac{m+1}{m}}, \quad (2.5)$$

$$\phi_i^* = \sum_{j=1}^3 \sum_{n=1}^{N_i} \frac{\eta_{i,n}^{dev}}{\alpha_{i,n}} ([\exp(\dot{e}_{ij}^v)]^{\alpha_{i,n}} - 1) + \frac{\eta_i^{vol}}{2} (\dot{\theta}_i^v)^2, \quad (2.6)$$

Table 1
Soft tissue material properties

| | GM | WM | BSCC |
|---|-----------------|-----------------|-----------------|
| Mass density (kg/m ³) | 1040 | 1040 | 1040 |
| <i>Elastoplastic response</i> | | | |
| Ogden's coefficient μ_1 (kPa) | -2.72 | -3.28 | -4.64 |
| Ogden's coefficient α_1 | -5.00 | -5.00 | -5.00 |
| Long-term shear modulus μ^∞ (kPa) | 6.80 | 8.20 | 11.60 |
| Bulk modulus κ (kPa) | 2190 | 2190 | 2190 |
| Yield stress σ_0 (kPa) | 20.0 | 20.0 | 20.0 |
| Reference plastic strain e_0^p | 0.05 | 0.05 | 0.05 |
| Hardening exponent n | 10 | 10 | 10 |
| Reference plastic strain rate \dot{e}_0^p | 0.001 | 0.001 | 0.001 |
| Plastic strain rate exponent m | 10 | 10 | 10 |
| Void density N_v (m ⁻³) | 10 ⁸ | 10 ⁸ | 10 ⁸ |
| Initial void radius a_0 (μ m) | 100 | 100 | 100 |
| <i>First viscoelastic mechanism</i> | | | |
| Relaxation time τ_1 (s) | 0.008 | 0.008 | 0.008 |
| Ogden's coefficient $\mu_{1,1}$ (kPa) | -1.36 | -1.64 | -2.32 |
| Ogden's coefficient $\alpha_{1,1}$ | -5.00 | -5.00 | -5.00 |
| Bulk modulus κ_1 (kPa) | 2190 | 2190 | 2190 |
| <i>Second viscoelastic mechanism</i> | | | |
| Relaxation time τ_2 (s) | 0.15 | 0.15 | 0.15 |
| Ogden's coefficient $\mu_{2,1}$ (kPa) | -1.36 | -1.64 | -2.32 |
| Ogden's coefficient $\alpha_{2,1}$ | -5.00 | -5.00 | -5.00 |
| Bulk modulus κ_2 (kPa) | 2190 | 2190 | 2190 |
| Initial shear modulus μ^0 (kPa) | 13.60 | 16.40 | 23.20 |

GM = gray matter; WM = white matter; BSCC = brain stem and corpus callosum.

Table 2
Skull and CSF properties

| | Skull | CSF |
|-----------------------------------|-------|------|
| Mass density (kg/m ³) | 1210 | 1004 |
| Shear modulus μ (kPa) | 3280 | 0.50 |
| Bulk modulus κ (kPa) | 4760 | 2190 |

which rule the time evolution of plastic and viscous internal forces; the reader should refer to Eqs. (2.35) and (2.36) in [7] for the relationship between the kinetic potentials and their duals. In (2.5) and (2.6), m is the plastic rate sensitivity exponent; \dot{e}_0^p is the reference plastic strain rate; \dot{e}_{ij}^v and $\dot{\theta}_i^v$ are the shear and volumetric viscous strain rates of the viscoelastic mechanisms; and $\eta_{i,n}^{dev}$, η_i^{vol} are shear and volumetric viscosities, respectively. Microinertia due to expanding voids is also included, as described in [7,41].

At thermodynamic equilibrium, the internal forces in the viscoelastic networks are relaxed and the material behavior is ruled by the sole elastoplastic response. When the material is away from equilibrium, the current viscoelastic strain can be regarded as a measure of transient shear tissue damage.

3. Finite element modeling of the human head

The injury simulations presented in this work make use of a finite element model of the human head recently developed at the Bioengineering Laboratory of the University of Salerno [6].

A finite element mesh was reconstructed from the axial Magnetic Resonance Images available in "The Whole Brain Atlas" of the Harvard Medical School (<http://www.med.harvard.edu/AAN-LIB/>), via 3D image processing and editing, using the commercial software Mimics (Materialise Group, Leuven, Belgium). The mesh

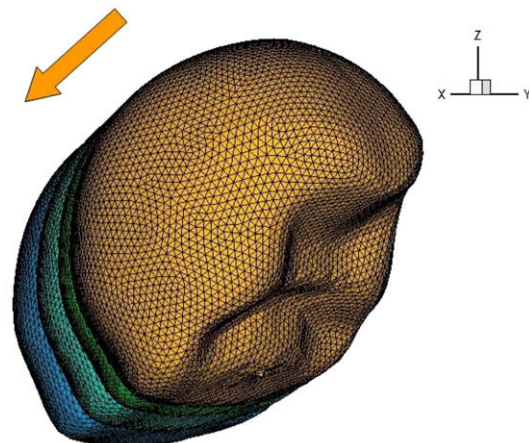


Fig. 3. Snap shots of the translational head motion following frontal impact ($t = 2, 4, 6, 8$ ms).

includes the following components (refer to Fig. 2): (1) skull without facial bones; (2) cerebrospinal fluid (CSF) in the form of a 3-mm thick layer; (3) gray matter; (4) white matter; (5) cerebellum; (6) corpus callosum; (7) telencephalic nuclei; (8) brain stem; (9) ventricles.

The entire model comprises 39047 tetrahedral composite elements [38], and is characterized by a detailed level similar to that of the Wayne State Brain Injury Model [45]. The model resolves the

smallest geometrical features (with exception of the finer structure of the cerebral cortex) with at least a few elements. Furthermore, the simulations were performed with 10-noded composite tetrahedra, and therefore we believe that the discretization error plays no significant role. The brain measures 1508 cm³ in volume (CSF excluded) and has a mass of 1.40 kg. The modeled portion of the skull is 678 cm³ in volume and has a mass of 0.82 kg. We refer the reader to [6] for further details about mesh geometry, density, and topology.

We employed the constitutive model described in the previous section for the brain tissue components, considering two viscoelastic mechanisms and one-term Ogden functions. Viscoelastic material properties frequently used in the literature for head injury simulations (cf. Zhou et al. [45], Zhang et al. [43,44], Kleiven [17], Kleiven and von Holst [16], Horgan and Gilchrist [14]) were suit-

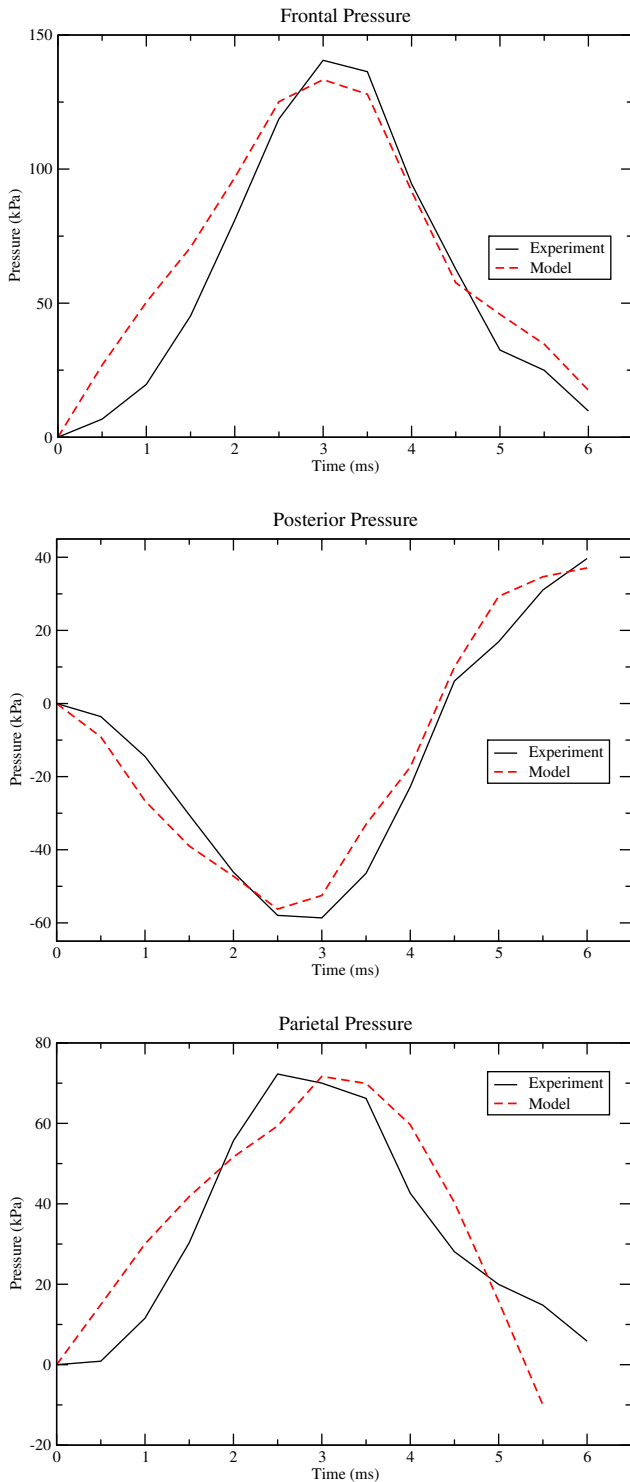


Fig. 4. Predicted vs experimental intracranial pressure time-histories [28, experiment no. 37].

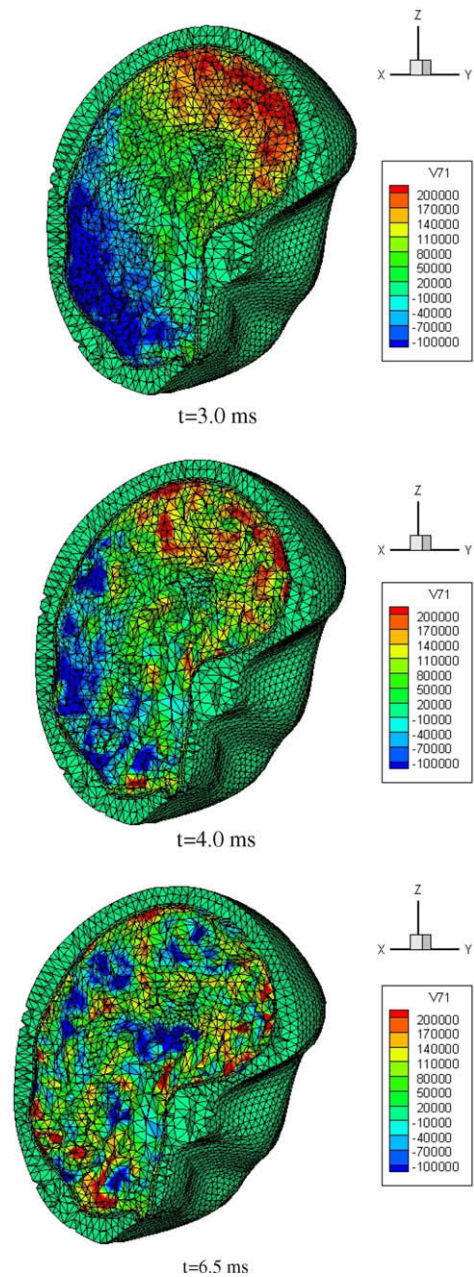


Fig. 5. Frontal impact: intracranial pressure contours (Pa).

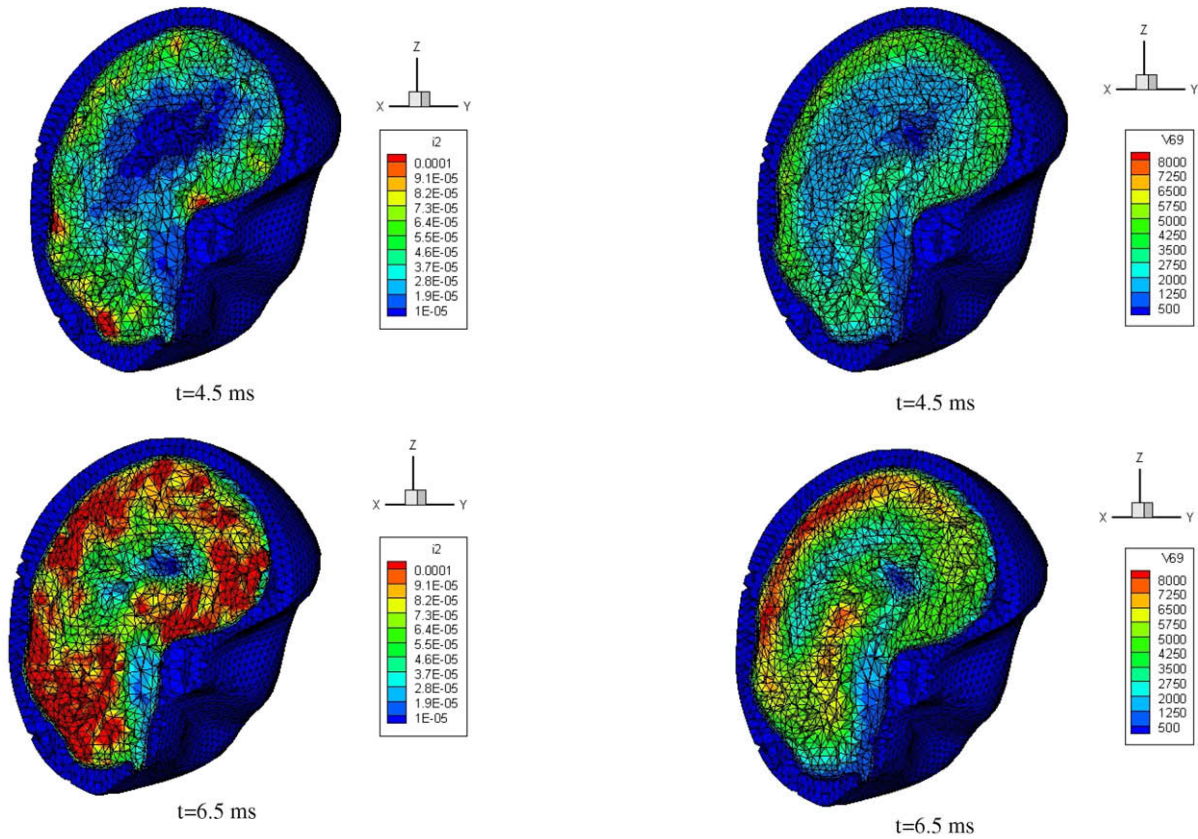


Fig. 6. Frontal impact: cavitation damage (dP) predictions.

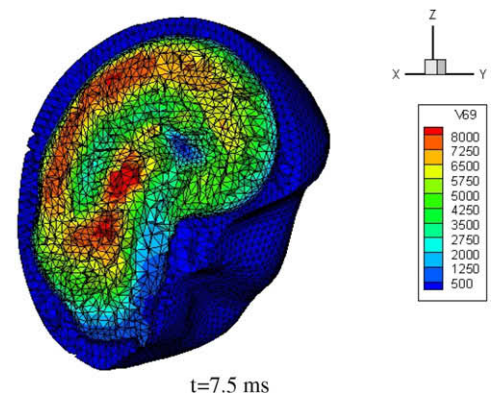


Fig. 7. Frontal impact: shear stress contours (Pa).

ably adapted to the present model.¹ We scaled by a factor of 1/2.5 the short-term shear moduli given by Zhang et al. [44] for white matter, gray matter, and brain stem, to ensure consistency with the short-term brain tissue model proposed by Mendis et al. [22]. In particular, we assigned shear stiffness ratios of 1/2, 1/4, 1/4 to the elastoplastic and the viscoelastic networks, respectively. Following the results given in [7,8], we considered negative $\{\mu, \alpha\}$ couples. We also adopted a yield stress of 20 kPa, amplifying by a factor of 2 the shear stress threshold defined by Zhang et al. [44] as a tolerable level for 80% probability of mild traumatic brain injury. The first approximation to the actual yield stress of brain tissue is due to the current lack of extensive experimental results in terms of plastic behavior, permanent deformation and regional dependence of damage properties in the brain tissue. This approximation proves to be reasonable as seen in Section 4.1.

The volumetric viscosities η_i^{vol} were set to zero, assuming purely elastic volumetric behavior in the viscoelastic networks, while the shear (deviatoric) viscosities $\eta_{i,n}^{dev}$ were expressed in terms of the relaxation times $\tau_i = \eta_i^{dev} / \mu_i$, where η_i^{dev} and μ_i are linear viscosities and shear moduli. We prescribed $\tau_1 = 0.008$ s in the first, and $\tau_2 = 0.15$ s in the second mechanisms [22]. The first mechanism accounts for short-term viscoelastic response and essentially controls time effects in impact problems (cf. next section). The complete set of material properties employed for soft tissue components is given in Table 1. As for the skull and the CSF, we adopted the hyperelastic models described in Table 2 which correspond to those adapted by Zhang et al. [43]. Free boundary conditions were assumed in accordance to the literature (cf. Zhou et al.

[46], Kleiven and von Holst [16], Horgan and Gilchrist [14]) and due to the short duration of the impact.

4. Impact simulations

The present section illustrates two different head injury simulations concerning a frontal and oblique head impacts with an external object. In the first case, validation is established with available experimental results. Attention is focused on intracranial pressures, shear stresses, and related brain tissue damage.

4.1. Frontal impact

We simulated experiment no. 37 by Nahum et al. [28] on the intracranial pressure dynamics in a human cadaver impacted by a rigid mass. The impact was not modeled via contact, however, it was reproduced by applying the experimental pressure

¹ Remark: The decision to refer to modeling papers for material properties, and not to experimental studies on swine or human brain tissue (like those presented in [9,27,23,24,34,39]), is due to the fact that the latter often do not account for very high strain rates comparable to those observed in traumatic brain injuries.

load-history over a frontal region of the skull, with semi-sinusoidal time distribution for a duration of 6 milliseconds and a peak force of 7.90 kN [28] (Fig. 3). The impact direction n had components $n_x = 0.0166$, $n_y = -0.8060$ and $n_z = 0.5917$ with respect to the global Cartesian frame X, Y, Z shown in Fig. 3. Similar simulations have been performed by other authors for validation of different finite element models (cf., e.g., Ruan et al. [36], Zhou et al. [45], Kleiven and von Holst [16], Horgan and Gilchrist [14]).

Fig. 4 shows the predicted pressure time-histories in three different brain regions (frontal, posterior-fossa and parietal lobes)

versus the corresponding experimental results given in [28]. A very good correlation between the model and experiment is observed; peak values and time distribution of the intracranial pressure partially validate the present constitutive and finite element models.

During the simulation, as well as in the referenced experiment by [28], positive (compressive) peak pressures were observed in the frontal brain region beneath the impact site, together with negative (tensile) pressure in the posterior-fossa area opposite to the impact site (Fig. 4). Those peaks approximately occurred in correspondence with the peak of the external pulse ($t = 3$ ms). After that time, the frontal pressure started to decrease toward zero, while the posterior pressure began to increase toward positive values. A pressure profile similar in shape to that of the frontal region, but reduced in amplitude, was observed in correspondence with the parietal lobe region (Fig. 4).

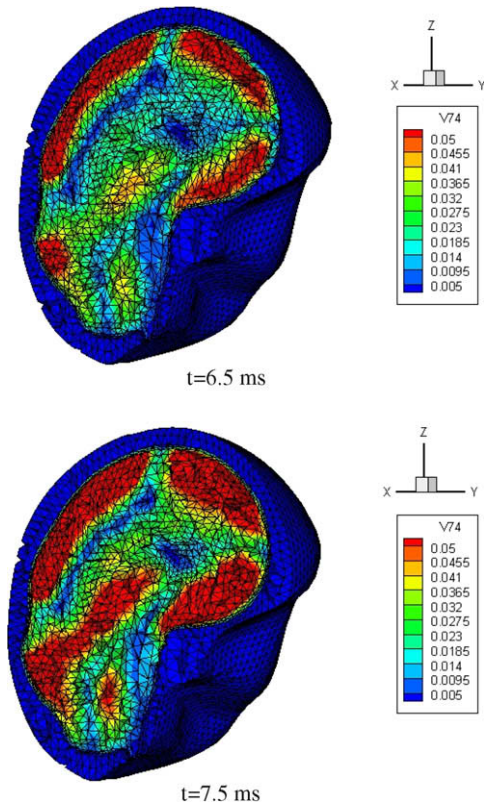


Fig. 8. Frontal impact: viscous shear deformation predictions.

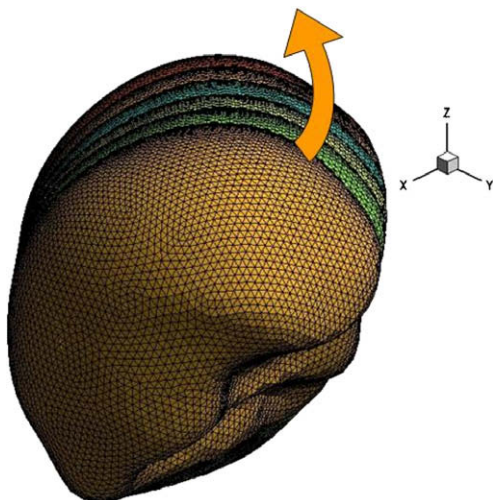


Fig. 9. Snap shots of the translational-rotational head motion following oblique impact ($t = 2, 4, 5, 6, 7, 8$ ms).

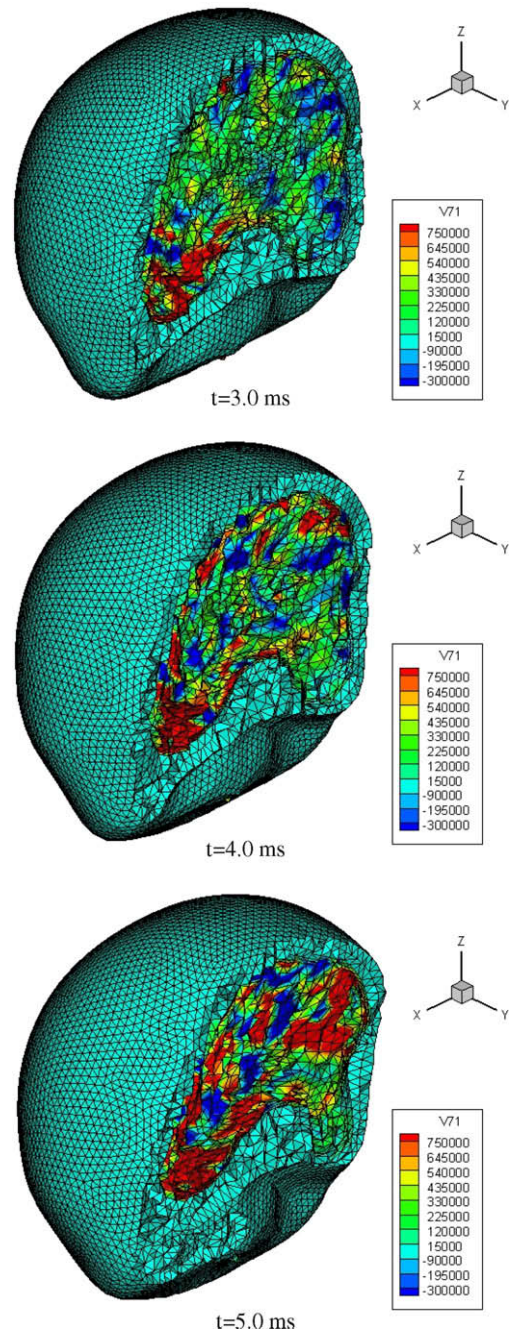


Fig. 10. Oblique impact: intracranial pressure contours (Pa).

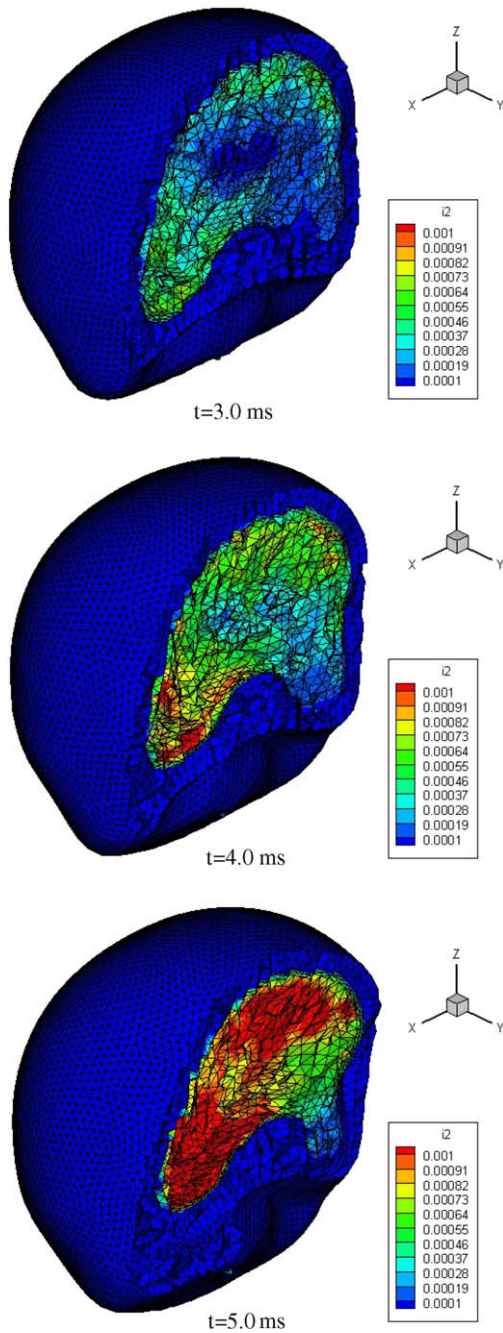


Fig. 11. Oblique impact: cavitation damage (θ^p) predictions.

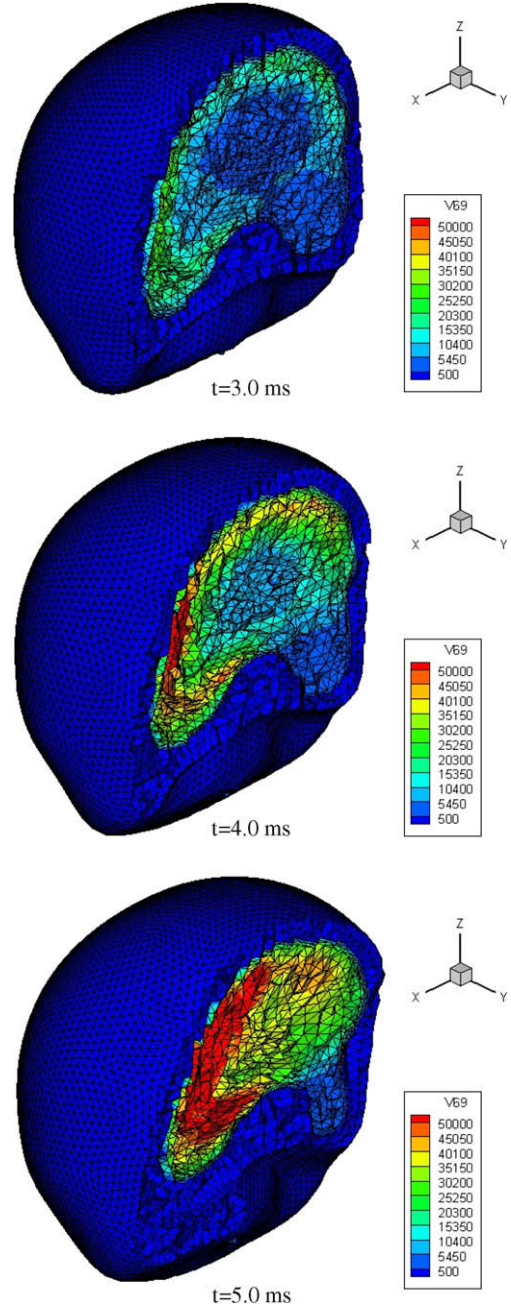


Fig. 12. Oblique impact: shear stress contours (Pa).

Contour plots of the intracranial pressure over a mid-sagittal section of the head model are shown in Fig. 5 at the peak ($t = 3$ ms), during the decreasing phase ($t = 4.5$ ms), and soon after the end of the pulse ($t = 6.5$ ms). One observes that the traveling stress wave reflects against the skull at the contrecoup site and then moves back toward the interior of the parenchyma. It is then followed by a tensile “tail” (negative pressure wave), which produces irreversible cavitation damage (volumetric plastic strain θ^p) in different brain regions, especially within the contrecoup region (Fig. 6). Cavitation initiates when the traveling tensile stress reaches a threshold value p_c (critical cavitation pressure) [41,40,7], and determines instable growth of voids in the tissue. This phenomenon is locally amplified by the superposition of primary and reflected tensile waves.

The dynamics of the shear deformation are slightly different. Fig. 7 shows contour plots, at different times, of the total effective shear stress τ , which continues to rise after the peak of the pulse. It is observed that the shear stress assumes extreme values at the parietal lobe, the corpus callosum, the thalamus, and the midbrain (cf. Zhang et al. [43,44], Horgan and Gilchrist [14]). Its highest value, however, remains below the adopted plastic threshold ($\tau \leq \sigma_0 = 20$ kPa, cf. Fig. 7), and hence no permanent shear damage is predicted by our model in the present case. Nevertheless, remarkable elastic and viscous shear deformations arise in different brain regions. Contour plots of the viscous shear strain ϵ^v in the first viscoelastic mechanism are depicted in Fig. 8. In the current example, ϵ^v can be regarded as a measure of transient (axonal) shearing damage of brain tissue, which will be released after the end of the pulse in a time duration sufficiently larger than the

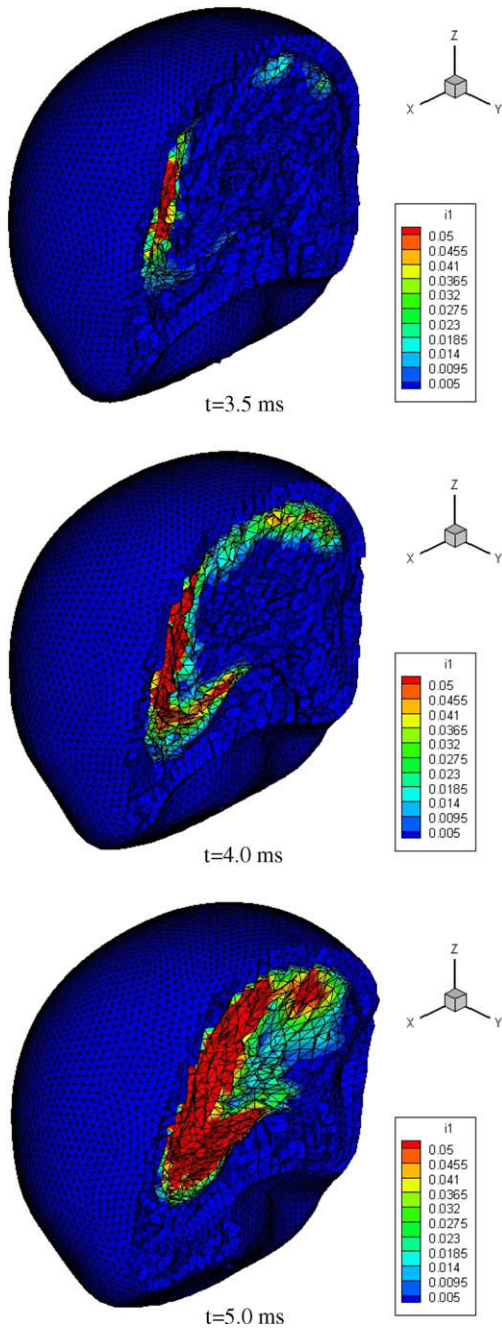


Fig. 13. Oblique impact: permanent shear damage predictions.

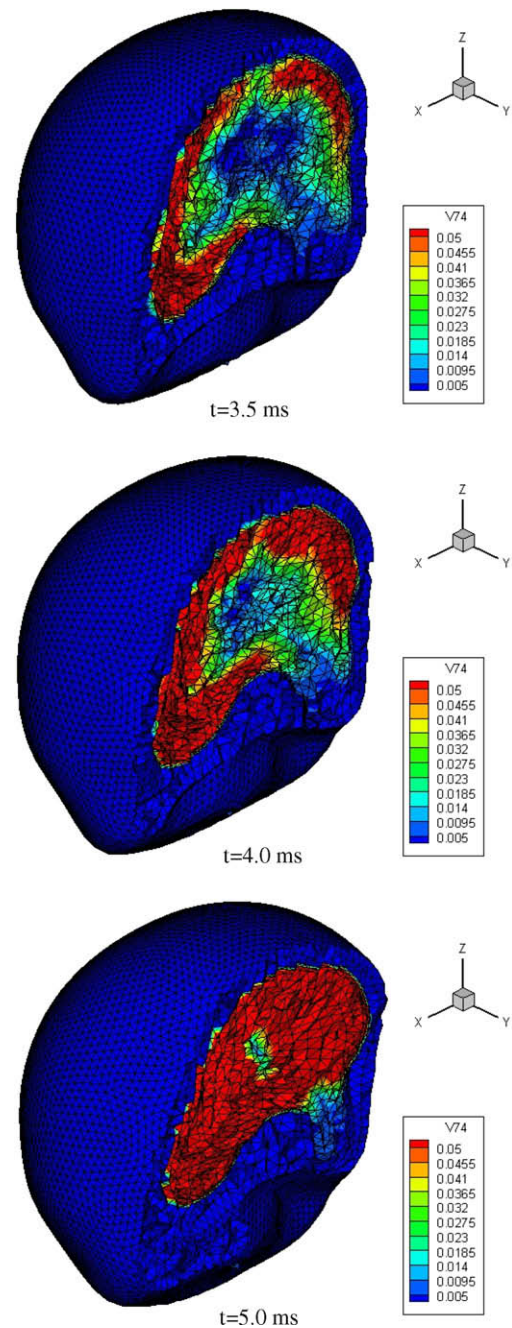


Fig. 14. Oblique impact: viscous shear deformation predictions.

relaxation time of the first viscoelastic mechanism ($t \gg 8$ ms, cf. Table 2).

4.2. Oblique impact

A predictive oblique impact event was simulated by applying the same pulse of the previous example on a lateral region of the frontal bone to induce a mixed translational–rotational motion of the head (Fig. 9). The impact direction was assumed to be inclined at 45° in the $X-Y$ plane (impact direction n components: $n_x = 0.707$, $n_y = -0.707$ and $n_z = 0$, cf. Fig. 9).

This predictive simulation resulted in the intracranial pressure profiles depicted in Fig. 10 over a section almost parallel to the impact direction through the center of the impact zone. One can observe markedly higher positive and negative pressures develop in

the present case within the coup and contrecoup regions, as compared to the case of a frontal impact. Such high intracranial pressures induce intense and diffused cavitation damage (Fig. 11), with peaks of θ^p being significantly higher than those observed in the previous example (cf. Fig. 6).

As for the shear stress τ , we recorded the time-history represented in Fig. 12. It can be noticed that the τ profiles extend within the brain as concentric circular ripples moving inward from the point of impact, thus qualitatively reproducing the contours of the velocity gradient associated with the rotational motion of the head (Fig. 9). Its peaks initially appear beneath the cortical surface, and then evolve toward the core regions of the brain (cf. Zhang et al. [44]). The shear stress values are up to 10 times higher than those predicted in the frontal impact case, which implies the attainment of the yield limit in the elastoplastic network and the

development of permanent shear damage ϵ^p , as shown in Fig. 13. Therefore, occurrence of DAI can be predicted, evolving from the periphery to the core of the brain. Viscous shear deformation ϵ^v in the first viscoelastic mechanism is also observed, with analogous time–space distribution to ϵ^p (Fig. 14). In the present case, the difference $\epsilon^v - \epsilon^p$ may be regarded as a measure of transient axonal shearing.

5. Conclusions

We have illustrated that clinically relevant injuries, such as DAI and cavitation, can be related to specific mechanical damage modes of brain tissue, which involve plastic and/or viscous deformation. A constitutive model capable of capturing observed types of damage mechanisms was utilized in two finite element simulations of TBIs in order to predict the distribution, intensity and reversibility/irreversibility of tissue damage indicators. A partial validation of the employed finite element model has been carried out, comparing numerical predictions of intracranial pressure with the outcomes of an experiment on a human cadaver impacted by a rigid mass. The same experiment is largely used in the biomechanical literature for validation of finite element models of the human head [14,16,36,46]. The determination of reliable plastic threshold parameters and viscoelastic material properties remains an open question for experimentalists to explore and modelers to utilize. Future directions of this work should include secondary cell-damage and may lead to the study of the correlation between mechanical damage of brain tissue and physiological brain dysfunction and the formulation of head injury criteria for medical, governmental and industrial applications. These types of studies, which must be carried out through collaborative mechanical–medical research, should address the definition of clinical–biomechanical injury tolerances, biomechanical–clinical correlation studies, computer and laboratory-based accident reconstruction, and micromechanical approaches. Validation of the model against in vivo behavior of brain tissue can be carried out simulating, for example, in vivo indentation tests on swine tissue, as done in Miller et al. [25]. Comparison between in vivo and in vitro experimental results could lead one to understand the existing relationship between material parameter values in the two cases. Also, the CSF skull–brain interface is often modeled either through linear elastic solid elements with low shear modulus, or via contact algorithms (cf., e.g., Kleiven [17] and references therein); CSF viscosity could be thought to not strongly influence the short-term response of the head model to impact events with duration of a few milliseconds. Nevertheless, a specific study about the CSF viscosity effects on head trauma is left as future work.

Acknowledgements

The support of the Regione Campania, Italy, through the program “Modeling Shape, Structure and Mechanical Behavior of the Skull–Encephalon Complex” is greatly acknowledged. The authors also want to sincerely thank Davide Zuppa, graduate student at the Department of Civil Engineering of the University of Salerno, for his relevant and precious collaboration with the present work.

References

- [1] J.H. Adams, D.I. Graham, Diffuse brain damages in non-missile head injury, in: Recent Advances in Histopathology, Churchill Livingstone, Edinburgh, 1984.
- [2] J.S. Bergström, M.C. Boyce, Constitutive modeling of the time-dependent and cyclic loading of elastomers and application to soft biological tissues, *Mech. Mater.* 33 (2001) 523–530.
- [3] D.W.A. Brands, P.H.M. Bovendeerd, J.S.H.M. Wisman, On the potential importance of non-linear viscoelastic material modelling for numerical prediction of brain tissue response: test and application, *Stapp Car Crash J.* 46 (2002) 103–121.
- [4] D.W.A. Brands, G.W.M. Peters, P.H.M. Bovendeerd, Design and numerical implementation of a 3-d non-linear viscoelastic constitutive model for brain tissue during impact, *J. Biomech.* 37 (2004) 127–134.
- [5] C.E. Brennen, Cavitation in biological and bioengineering contexts, in: Fifth International Symposium on Cavitation, Osaka, Japan, 2003.
- [6] L. Cardamone, Analisi numerica del trauma cranico da impatto, Technical report, Bioengineering Laboratory, University of Salerno, Italy, 2005.
- [7] T. El Sayed, A. Mota, F. Fraternali, M. Ortiz, A variational constitutive model for soft biological tissues, *J. Biomech.* 41 (7) (2008) 1458–1466.
- [8] T. El Sayed, Constitutive models for polymers and soft biological tissues, Ph.D. thesis, California Institute of Technology, 2007.
- [9] G. Franceschini, D. Bigoni, P. Regitnig, G.A. Holzapfel, Brain tissue deforms similarly to filled elastomers and follows consolidation theory, *J. Mech. Phys. Solids* 54 (12) (2006) 2592–2620.
- [10] S. Fujiwara, Y. Yanagida, Y. Mizoi, Impact induced intracranial pressure caused by an accelerated motion of the head or by skull deformation: an experimental study using physical models of the head and neck and bones of the skull, *Forensic Sci. Int.* 43 (1989) 159–169.
- [11] T.C. Gasser, G.A. Holzapfel, A rate-independent elastoplastic constitutive model for biological fiber-reinforced composites at finite strains: continuum basis, algorithmic formulation and finite element implementation, *Comput. Mech.* 29 (2002) 340–360.
- [12] A.G. Gross, A new theory on the dynamics of brain concussion and brain injury, *J. Neurosurg.* 15 (1958) 548–561.
- [13] W.N. Hardy, T.B. Khalil, A.I. King, Literature review of head injury biomechanics, *Int. J. Impact Engrg.* 15 (1994) 561–586.
- [14] T.J. Horgan, M.D. Gilchrist, The creation of three-dimensional finite element models for simulating head impact biomechanics, *Int. J. Crashworthiness* 8 (2003) 353–366.
- [15] E.A.C. Johnson, P.G. Young, The analysis of pressure response in head injury, in: C2006 Digital Human Modeling for Design and Engineering Conference, July 2006, Lyon, France, 2006. SAE paper no. 2006-01-2368.
- [16] S. Kleiven, H. von Holst, Consequence of head size following trauma to the human head, *J. Biomech.* 35 (2002) 153–160.
- [17] S. Kleiven, Finite element modeling of the human head, Ph.D. thesis, Royal Institute of Technology, Stockholm, Sweden, 2002.
- [18] J.E. Leestma, Forensic Neuropathology, Raven Press, NY, 1987.
- [19] S. Lindgreen, L. Rinder, Experimental studies in head injury. II. pressure propagation in percussion–concussion, *Biophys. J.* 3 (1966) 174–180.
- [20] P. Lubock, W. Goldsmith, Experimental cavitation studies in a model headneck system, *J. Biomech.* 13 (1980) 1041–1052.
- [21] D.F. Meaney, Relationship between structural modeling and hyperelastic material behavior: application to CNS white matter, *Biomech. Model. Mechanobiol.* 1 (2003) 279–293.
- [22] K.K. Mendis, R.L. Stalnaker, S.H. Advani, A constitutive relationship for large deformation finite element modeling of brain tissue, *J. Biomech. Engrg.* 117 (1995) 279–285.
- [23] K. Miller, K. Chinzei, Constitutive modeling of brain tissue: experiment and theory, *J. Biomech.* 30 (1997) 1115–1121.
- [24] K. Miller, K. Chinzei, Mechanical properties of brain tissues in tension, *J. Biomech.* 35 (2002) 483–490.
- [25] K. Miller, K. Chinzei, G. Orssengo, P. Bednarsz, Mechanical properties of brain tissue in vivo: experiment and computer simulation, *J. Biomech.* 43 (2000) 1369–1376.
- [26] K. Miller, W. Taylor, A. Wittek, Mathematical models of brain deformation behaviour for computed–integrated neurosurgery, in: Research Report of Intelligent Systems for Medicine Laboratory, University of Western Australia, 2006. ISML/01/06.
- [27] K. Miller, Method of testing very soft biological tissues in compression, *J. Biomech.* 38 (2005) 153–158.
- [28] A.M. Nahum, R.W. Smith, C.C. Ward, Intracranial pressure dynamics during head impact, in: Proceedings of the 21st Stapp Car Crash Conference, 1977. SAE paper no. 770922.
- [29] G.S. Nusholtz, L.G. Glascoe, E.B. Wylie, Modeling cavitation during head impact, in: Proceedings of NATO/AGARD Head Impact Conference, Paper 6, 1996.
- [30] R.W. Ogden, Non-linear Elastic Deformations, Ellis Horwood, Chichester, UK, 1984.
- [31] M. Ortiz, A. Molinari, Effect of strain-hardening and rate sensitivity on the dynamic growth of a void in a plastic material, *J. Appl. Mech.-Trans., ASME* 59 (1) (1992) 48–53.
- [32] M. Ortiz, L. Stainier, The variational formulation of viscoplastic constitutive updates, *Comput. Methods Appl. Mech. Engrg.* 171 (3–4) (1999) 419–444.
- [33] S.J. Perles, N.B. Rewcastle, Shear injuries of the brain, *Can. Med. Assoc. J.* 96 (1967) 577–582.
- [34] M.T. Prange, S.S. Margulies, Regional, directional, and age dependent properties of the brain undergoing large deformation, *J. Biomech. Engrg.-Trans., ASME* 124 (2002) 244–252.
- [35] S.R. Rodrigues, E.A.C. Johnson, P.G. Young, The influence of projectile mass and velocity on the response of the brain to blunt impact, in: BioMECH 2003, Rhodes, Greece, 2003.
- [36] J.S. Ruan, T.B. Khalil, A.I. King, Dynamic response of the human head to impact by three-dimensional finite element analysis, *J. Biomech. Engrg.* 116 (1994) 44–50.
- [37] S.J. Strich, Diffuse degeneration of cerebral white matter in severe dementia following head injury, *J. Neurol. Neurosurg. Psychiatry* 19 (1956) 163–185.

- [38] P. Thoutireddy, J.F. Molinari, E.A. Repetto, M. Ortiz, Tetrahedral composite finite elements, *Int. J. Numer. Methods Engrg.* 53 (2002) 1337–1351.
- [39] F. Velardi, F. Fraternali, M. Angelillo, Anisotropic constitutive equations and experimental tensile behaviour of brain tissue, *Biomech. Model. Mechanobiol.* 5 (2006) 53–61.
- [40] K. Weinberg, M. Ortiz, Shock wave induced damage in kidney tissue, *Comput. Mater. Sci.* 32 (2005) 588–593.
- [41] K. Weinberg, A. Mota, M. Ortiz, A variational constitutive model porous metal plasticity, *Comput. Mech.* 37 (2006) 142–152.
- [42] Q. Yang, L. Stainer, M. Ortiz, A variational formulation of the coupled thermo-mechanical boundary-value problem for general dissipative solids, *J. Mech. Phys. Solids* 54 (2006) 401–424.
- [43] L. Zhang, K.H. Yang, A.I. King, Comparison of brain responses between frontal and lateral impact by finite element modeling, *J. Neurotraum.* 18 (2001) 21–30.
- [44] L. Zhang, K.H. Yang, A.I. King, A proposed injury threshold for mild traumatic brain injury, *J. Biomech. Engrg.-Trans., ASME* 126 (2004) 226–236.
- [45] C. Zhou, T.B. Khalil, A.I. King, A new model comparing impact response of the homogeneous and inhomogeneous human brain, in: *Proceedings of the 39th Stapp Car Crash Conference*, 1995. SAE paper no. 952714.
- [46] C. Zhou, T.B. Khalil, A.I. King, A new model comparing impact response of the homogeneous and inhomogeneous human brain, in: *Proceedings of the 39th Stapp Car Crash Conference*, SAE J. Automot. Engrg. 952714, 1995, pp. 121–137.